Chemical Science

Accepted Manuscript

This article can be cited before page numbers have been issued, to do this please use: J. Li, G. Ke, M. Yang, G. Lv, L. Cao, W. Li, T. Han, W. Wang, Y. Zhou and H. He, *Chem. Sci.*, 2026, DOI: 10.1039/D5SC08541A.

ROYAL SOCIETY OF CHEMISTRY

rsc.li/chemical-science

View Article Online
DOI: 10.1039/D5SC08541A

The relevance of Cr defects and photoelectrochemical water oxidation activity of monoclinic $PbCrO_4$ films

Jiahe Li,[a] Gaili Ke,[a] Minji Yang,[b] Guoliang Lv,[a] Lanyi Cao,[a] Wenjun Li,[a] Tao Han,[a] Wenrong Wang,[a] Yong Zhou[c] and Huichao He[a]*

[a]College of Materials and New Energy, Chongqing University of Science and Technology. Chongqing 401331, China.

[b]Synthetic Lubricant Oil and Grease Branch, Sinopec Lubricant *Co.*, *Ltd.*, Chongqing, 400039, China.

[c]Ecomaterials and Renewable Energy Research Center, School of Physics, University Nanjing, Nanjing 211102, China

*Corresponding Author

Email: hehuichao@cqust.edu.cn

View Article Online
DOI: 10.1039/D5SC08541A

Abstract: The presence of Cr defects in monoclinic $PbCrO_4$ is closely related to its solar water oxidation activity, which be overlooked in the preparation of $PbCrO_4$ films and unrevealed in the researches of $PbCrO_4$ photoanodes. Herein, monoclinic $PbCrO_4$ films with few Cr defects ($PbCrO_4$-F_{VCr}) were prepared on FTO substrate through covering the drop-coating Pb^{2+}/Cr^{3+} precursor solution to reduce the loss of Cr during thermal treating. Relative to the monoclinic $PbCrO_4$ films with rich Cr defects ($PbCrO_4$-R_{VCr}), higher solar water oxidation activity was achieved on the $PbCrO_4$-F_{VCr} films as photoanodes. At 1.23 V *vs.* RHE, a higher water oxidation photocurrent of 1.13 mA cm^{-2} was produced on the $PbCrO_4$-F_{VCr} film photoanodes, which is two-fold to the $PbCrO_4$-R_{VCr} film photoanodes (0.55 mA cm^{-2}). Meanwhile, the $PbCrO_4$-F_{VCr} film photoanodes had faster water oxidation kinetics than $PbCrO_4$-R_{VCr} film photoanodes. The water oxidation rate constant (k_{O2}) on the $PbCrO_4$-F_{VCr} film photoanodes was 40.6 s^{-1}, while a lower k_{O2} of 8.2 s^{-1} on the $PbCrO_4$-R_{VCr} film photoanodes. Experimental detections and theoretical calculations jointly revealed that $PbCrO_4$ films with fewer Cr defects being of higher solar water oxidation activity can be attributed to following reasons: (i) the presence of Cr defects can result in the formation of deep energy level in $PbCrO_4$, which is unfavorable to carrier transfer in the bulk of $PbCrO_4$ films; (ii) the presence of Cr defects can cause the formation of unsaturated O dangling bonds on $PbCrO_4$, which are harmful traps for carrier separation on the surface of $PbCrO_4$ films; (iii) Cr has a half-filled $3d^5$ orbital to provide active sites for reaction, the presence of Cr defects weakens the catalytic activity of $PbCrO_4$ for water oxidation, and turns the rate-limiting step to the dehydrogenation of *OH into *O which requires a high energy barrier of 1.88 eV. The present work provides insight into monoclinic $PbCrO_4$ film photoanodes from the relevance of preparation condition, Cr defects, water oxidation activity and reaction mechanism.

Keywords: $PbCrO_4$ photoanode; Cr defects; Solar water oxidation

View Article Online
DOI: 10.1039/D5SC08541A

1. Introduction

N-type monoclinic $PbCrO_4$ has a similar electronic structure to monoclinic $BiVO_4$, [1] it has been investigated as a photoanode material for photoelectrochemical (PEC) water splitting in recent years. [2-7] Based on its advantageous band gap (~ 2.2 eV) and valence band position (~2.2 V vs. RHE), [2] monoclinic $PbCrO_4$ could harvest ~20% of solar energy to drive water oxidation theoretically. [8] However, the previously reported $PbCrO_4$ photoanodes' activity is far less than the theoretical expectation, due to the presence of high carrier recombination and sluggish water oxidation kinetics. As is well known, the composition and structure of materials jointly determine their properties and related performance. The presence of defects in semiconductors could impact their electronic structure, carrier separation and migration behavior, thereby changing photocatalytic and PEC activity obviously. [9, 10] For monoclinic $PbCrO_4$, its Cr^{6+} is located at the center of CrO_4 tetrahedron, and Pb^{2+} is surrounded by 8-9 oxygen atoms due to its lone pair electron effect.[11, 12] From the perspectives of electronic structure, one Cr defect carries three effective negative charges (V_{Cr}''') in $PbCrO_4$. In theory, the presence of high-concentration Cr defects could disrupt the CrO_4 tetrahedron network and form unsaturated O dangling bonds as well as defect-level traps, which are disadvantageous to the delocalization separation and transfer of electrons/holes.

Significantly, drop/spin-coating combined with thermal treating is the common approach for the preparation of monoclinic $PbCrO_4$ film. Typically, Li *et al.* used spin-coating/thermal treating method to prepare $PbCrO_4$ films on fluorine-doped tin oxide coated glass (FTO), and invented acetylacetone and poly (ethylene glycol) as dual ligands to regulate the nucleation and crystal growth of monoclinic $PbCrO_4$ films. [4, 6] Cho *et al.* prepared $PbCrO_4$ films on FTO using drop-coating/thermal treating approach, and found citric acid adding into precursor solution can stabilize Pb^{2+} and Cr^{3+} as well as suppress

View Article Online
DOI: 10.1039/D5SC08541A

them segregation to form smooth and fine monoclinic $PbCrO_4$ film. [5, 7] Although these pioneering investigations made significant contributions to the preparation of monoclinic $PbCrO_4$ films, the underlying influence of thermal treatment on the composition and structure of resultant $PbCrO_4$ films has been overlooked. During thermal treating at high temperature in air, the metal ions in precursor solution may be lost along with the pyrolysis of solvents, which could induce the formation of metal defects in resultant multi-metal oxides. In the preparation of $BiVO_4$ films using spray pyrolysis method, Lamers *et al.* found the loss of V during the VO^{3+}/Bi^{3+} precursor solution annealing above 500℃ in air, and observed the resultant $BiVO_4$ films with V defects and low carrier mobility. [13] It is worthy of special attention that Cr can be thermally evaporated at lower temperature (T>500°C) relative to Pb (T>600℃). The thermal evaporation of Cr from stainless steels at T>500°C has been extensively observed. [14] Thus, it is very possible that Cr defects are formed in monoclinic $PbCrO_4$ films using drop/spin-coating combined with thermal treating approach for synthesis. Several works have demonstrated that semiconductor photoelectrode materials with low-concentration defects usually have high crystallinity and can drive solar water splitting efficiently. [15-17] For the achievement of efficient solar water oxidation on $PbCrO_4$ film photoanodes, it is necessary and significant to suppress the formation of high-concentration Cr defects in monoclinic $PbCrO_4$ films during synthesis.

Herein, monoclinic $PbCrO_4$ films with few Cr defects ($PbCrO_4$-F_{VCr}) were prepared on FTO substrate through covering the drop-coating Pb^{2+}/Cr^{3+} precursor solution to reduce the thermal loss of Cr during annealing treatment. Compared with the monoclinic $PbCrO_4$ films with rich Cr defects ($PbCrO_4$-R_{VCr}) for solar water oxidation, a two-fold water oxidation photocurrent was produced on the $PbCrO_4$-F_{VCr} film photoanodes (1.13 mA cm^{-2} at 1.23 V *vs.* RHE). Meanwhile, faster water oxidation kinetics was achieved on the

View Article Online
DOI: 10.1039/D5SC08541A

$PbCrO_4$-R_{VCr} film photoanodes. The $PbCrO_4$-F_{VCr} film photoanodes had a water oxidation rate constant (k_{O2}) of 40.6 s^{-1}, which is ~5 times for the k_{O2} of the $PbCrO_4$-R_{VCr} film photoanodes (8.2 s^{-1}). Based on experimental detections and DFT calculations, $PbCrO_4$ films with fewer Cr defects being of higher activity can be ascribed as following reasons: (i) the presence of Cr defects can result in the formation of deep energy level in $PbCrO_4$, which is unfavorable to carrier transfer in the bulk of $PbCrO_4$ films; (ii) the presence of Cr defects can cause the formation of unsaturated O dangling bonds on $PbCrO_4$, which are harmful traps for carrier separation on the surface of $PbCrO_4$ films; (iii) Cr has a half-filled $3d^5$ orbital to provide active sites for reaction, the presence of Cr defects weakens the catalytic activity of $PbCrO_4$ for water oxidation, and turns the rate-limiting step to the dehydrogenation of *OH into *O which requires a high energy barrier of 1.88 eV.

2. Experimental section

2.1 Preparation of $PbCrO_4$-F_{VCr} and $PbCrO_4$-R_{VCr} films

The $PbCrO_4$-F_{VCr} and $PbCrO_4$-R_{VCr} films were prepared by drop-coating combined with thermal treating method (please see the diagram shown in **Fig. 1**). Typically, $Pb(NO_3)_2$ (AR, Aladdin) and $Cr(NO_3)_3$ (AR, Aladdin) were dissolved into 5 mL of distilled water to form 0.2 M Pb^{2+} and 0.2 M Cr^{3+} precursor solution, respectively. Then, 100 mg of polyethylene glycol (AR, Aladdin) was added into the Pb^{2+} precursor solution to stabilize Pb^{2+}, while 70 μL of acetylacetone (Aladdin, 99.8%) was dropped into the Cr^{3+} precursor solution to stabilize Cr^{3+}. After that, the Pb^{2+} and Cr^{3+} precursor solution was treated by ultrasonication at 60℃ for 30 min, respectively. Subsequently, the Pb^{2+} and Cr^{3+} precursor solution was mixed and diluted using ethylene glycol (AR, Kelong) to form 0.01 M Pb^{2+}/Cr^{3+} precursor solution. Finally, 200 μL of Pb^{2+}/Cr^{3+} precursor solution was dropped onto a clean FTO glass (10×20×2 mm,15Ω/sq), and thermally treated in a

View Article Online
DOI: 10.1039/D5SC08541A

muffle furnace (chamber: 20×30×20 cm) at 500℃ (heating rate: 2.5℃/min) for 2 h in air. For the preparation of $PbCrO_4$-F_{VCr} films, a culture dish (diameter: 6.0 cm; height:1.6 cm) was used to cover the Pb^{2+}/Cr^{3+} precursor solution during thermal treating. For comparison, $PbCrO_4$-R_{VCr} films were prepared not using culture dish cover during thermal treating for the Pb^{2+}/Cr^{3+} precursor solution.

To check the presence and content difference of O dangling bonds on the as-prepared $PbCrO_4$ films, $PbCrO_4$-F_{VCr} and $PbCrO_4$-R_{VCr} films were immersed in 0.01 M 1-octadecanethiol ($C_{18}H_{38}S$, 97%, Macklin) ethanol solution for 24 h to passivate their O dangling bonds. Then, two types of $PbCrO_4$ films were washed with deionized water for photocurrent measurements.

2.2 Characterizations of samples

The crystal structure, morphology and elemental chemical state of $PbCrO_4$-F_{VCr} and $PbCrO_4$-R_{VCr} films were checked using X-ray diffractometer (XRD, SmartLab-9kW, Rigaku), scanning electron microscopy (SEM, Regulus 8100), transmission electron microscope (TEM, Tecnai G220) and X-ray photoelectron spectroscopy (XPS, ESCALAB 250Xi), respectively. The UV-vis absorption spectrum of $PbCrO_4$-F_{VCr} and $PbCrO_4$-R_{VCr} films was measured on a HITACHI spectrophotometer (UH5700). The photoluminescence emission (PL) spectrum of $PbCrO_4$-F_{VCr} and $PbCrO_4$-R_{VCr} films was detected using a FLS1000 photoluminescence spectrometer. The electron paramagnetic resonance (EPR) spectrum of $PbCrO_4$-F_{VCr} and $PbCrO_4$-R_{VCr} films was recorded on a Bruker EPR spectrometer (EMPplus-10/12). The water-contacting angle of $PbCrO_4$-F_{VCr} and $PbCrO_4$-R_{VCr} films was observed through contact angle meter (SINDIN, SCD-100). Surface photovoltage and transient surface photovoltage spectrum of $PbCrO_4$-F_{VCr} and $PbCrO_4$-R_{VCr} films were detected using surface photovoltage spectroscopy (Beijing China Education Au-light *Co.*, *Ltd.*, CEL-TPV2000). For $PbCrO_4$-F_{VCr} and $PbCrO_4$-R_{VCr}

View Article Online
DOI: 10.1039/D5SC08541A

films before and after stability testing, their Raman spectrum was detected using Raman spectrometer (MultiRAM, Bruker).

2.3 Photoelectrochemical measurements

All of PEC measurements were conducted on a CHI 760e electrochemical workstation with a three-electrode cell at room temperature. The as-prepared $PbCrO_4$ films were used as working electrodes directly, the counter electrode was a Pt wire (99%), and the reference electrode was an Ag/AgCl electrode. The light source was a 300 W xenon lamp (Beijing China Education Au-light *Co.*, *Ltd.*) that equipped with a 1.5G filter to provide 100 mW cm^{-2} illumination. The PEC measurements were carried out using back-side illumination, namely the light firstly penetrated FTO then to $PbCrO_4$ film. 0.5 M phosphate buffer (PBS, pH 7.0) aqueous solution and 0.1 M potassium hydrogen phthalate (KHP)/0.5 M Na_2SO_3 mixing aqueous solution were used as electrolyte, respectively. The potential applied on working electrode was converted into RHE potential using following equation:

$$E_{RHE} = E_{Ag/AgCl} + 0.0592\,pH + 0.197 \quad (1)$$

where $E_{Ag/AgCl}$ is the applied potential, and pH is the pH value of electrolyte.

The charge separation (η_{sep}) and injection (η_{inj}) efficiency testing were performed in 0.5 M PBS/0.2 *vol.*% H_2O_2 electrolyte. The η_{sep} and η_{inj} of $PbCrO_4$-F_{VCr} and $PbCrO_4$-R_{VCr} film photoanodes were calculated according to following equations:

$$\eta_{sep} = \frac{J_{H_2O_2}}{J_{abs}} \times 100\% \quad (2)$$

$$\eta_{inj} = \frac{J}{J_{H_2O_2}} \times 100\% \quad (3)$$

where J_{abs} is the calculated photocurrent density based on the UV-vis absorption data of films (**Fig. 6a**), J_{H2O2} is the photocurrent density of film photoanodes in 0.5 M PBS/0.2 *vol.*% H_2O_2 (**Fig. S5**), J is photocurrent density film photoanodes in 0.5 M PBS.

The applied bias photon-to-current efficiency (ABPE) of $PbCrO_4$-F_{VCr} and $PbCrO_4$-

View Article Online
DOI: 10.1039/D5SC08541A

R_{VCr} film photoanodes was calculated by following equation:

$$ABPE = \frac{j(mA\ cm^{-2}) \times (1.23 - E_{RHE})}{100\ mW\ cm^{-2}} \times 100\% \quad (4)$$

where E_{RHE} is the applied potential *vs.* RHE, j is the photocurrent density of film photoanodes under AM 1.5G illumination.

The Mott-Schottky plots of $PbCrO_4$-F_{VCr} and $PbCrO_4$-R_{VCr} film photoanodes were recorded in a potential range of 0.3 to 0.5 V *vs.* RHE under AM1.5G illumination. The carrier concentration of $PbCrO_4$-F_{VCr} and $PbCrO_4$-R_{VCr} films was calculated using following equation:

$$1/C^2 = (2/e\varepsilon\varepsilon_0 A^2 N_d)(V_a - V_{fb} - kT/e) \quad (5)$$

where C is the capacitance, ε is the relative dielectric constant of $PbCrO_4$, ε_0 is the permittivity of vacuum (8.854×10^{-12} F cm^{-1}), k is the Boltzmann constant (1.381×10^{-23}J K^{-1}), e is the elemental charge (1.602×10^{-19} C), A is the surface area of sample, N_d is carrier concentration, V_a is the applied potential, V_{fb} is the flat band potential, and T is temperature.

The electrochemical impedance spectroscopy (EIS) measurements were performed at 1.23 V *vs.* RHE. The testing frequency ranged from 100000 to 0.01 Hz with an amplitude of 10 mV. The measured EIS data were fitted by Zview software under proposed equivalent circuit model. Based on the EIS Bode plots, the holes' lifetime (τ) on two types of $PbCrO_4$ film photoanodes was obtained by following equation:

$$\tau = \frac{1}{2}\pi f_m \quad (6)$$

where f_m is the maximum phase in frequency range.

The water oxidation rate constant (k_{O2}) and charge transfer rate constant (k_{tran}) of two types of $PbCrO_4$ film photoanodes were calculated on the basis of the fitted components' values of equivalent circuit (the values shown in **Table 2**).[18-21] k_{O2} was calculated through following equation:

View Article Online
DOI: 10.1039/D5SC08541A

$$k_{O2} = \frac{1}{R_{ct}\, CPE_{ct}} \quad (7)$$

k_{tran} was calculated by following equation:

$$k_{tran} = \frac{1}{R_{sc}\, CPE_{sc}} \quad (8)$$

where R_{ct} is the water oxidation resistance, R_{sc} is the charge transfer resistance, CPE_{ct} is the constant phase element of electrolyte/photoelectrode, and CPE_{sc} is the constant phase element of photoelectrode surface.

2.4 Density functional theory calculations

The charge density and the density of states of $PbCrO_4$(120) with and without Cr detects were calculated using Vienna Ab initio Simulation Package (VASP). [22, 23] The exchange-correlation potential was described by Perdew−Burke−Ernzerhof (PBE) generalized gradient approach (GGA). [24] The electron-ion interactions were accounted by projector augmented wave (PAW). [25] All density functional theory (DFT) calculations were performed with a cut-off energy of 400 eV, and 2×1×1 Gamma centered Monkhorst-Pack grids k-points were selected to sample in Brillouin zone integration. The energy and force convergence criteria of the self-consistent iteration were set to 10^{-4} eV and 0.05 eV $Å^{-1}$, respectively. DFT-D3 method was used to describe van der Waals (vdW) interactions. [26]

The Gibbs free energy changes (ΔG) of water oxidation on $PbCrO_4$(120) with and without Cr detects were calculated using the following formula:

$$\Delta G = \Delta E + \Delta \mathrm{ZPE} - T\Delta S + \Delta G_{\mathrm{U}} + \Delta G_{\mathrm{pH}} \quad (9)$$

where ΔE is the difference of electron energies calculated by DFT; ΔZPE and ΔS are the changes of zero-point energy and entropy, respectively, which are obtained from vibrational frequencies. T is the temperature (298.15 K). $\Delta G_{\mathrm{U}} = -eU$, here U is the applied electrode potential. $\Delta G_{\mathrm{pH}} = k_{\mathrm{B}}T \times ln\ 10 \times pH$, where k_{B} is the Boltzmann constant.

View Article Online
DOI: 10.1039/D5SC08541A

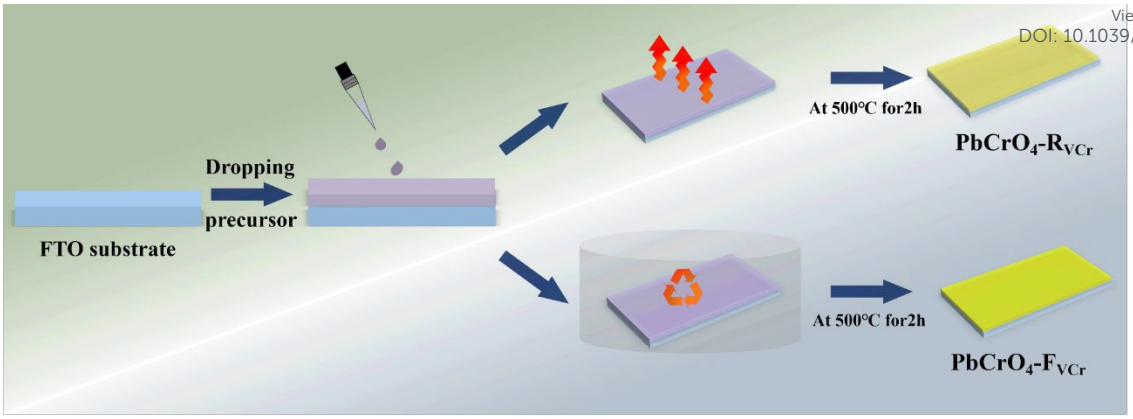

Fig. 1 The diagram of $PbCrO_4$-F_{VCr} and $PbCrO_4$-R_{VCr} film preparation.

3. Results and discussion

3.1 Characterization results

Fig. 2a to **f** show the typical SEM images of $PbCrO_4$-R_{VCr} and $PbCrO_4$-F_{VCr} films. From the top and sectional SEM images shown in **Fig. 2a**, **b** and **c**, it can be seen that $PbCrO_4$-R_{VCr} films are not dense and flat enough, and obvious gaps be formed and distributed in whole film evenly. By comparison, $PbCrO_4$-F_{VCr} films were denser and flatter, and few gaps were observed (**Fig. 2d, e** and **f**). In term of microscopic morphology, $PbCrO_4$-R_{VCr} and $PbCrO_4$-F_{VCr} films consisted of connective nanoparticles, but the nanoparticle size of $PbCrO_4$-R_{VCr} films (average size ~70 nm) was smaller than that of $PbCrO_4$-F_{VCr} films (average size ~100 nm) (**Fig. 2b**, **e** and **Fig. S1** in *Supplementary Information*). In general, $PbCrO_4$-R_{VCr} films (~230 nm, **Fig. 2c**) were slightly thicker than $PbCrO_4$-F_{VCr} films (~200 nm, **Fig. 2f**), due to their difference in morphology and evenness, although their preparation used the same amount of Pb^{2+}/Cr^{3+} precursor solution. In the HRTEM image of $PbCrO_4$-F_{VCr} films, the crystalline feature was observed and the lattice space was ~0.32 nm, which is corresponding to the typical crystal feature of $PbCrO_4$(120) (**Fig. 2g**). For the preparation of two types of $PbCrO_4$ films, the only condition difference was the presence and absence of culture dish covering above the Pb^{2+}/Cr^{3+} precursor solution during annealing treatment. During the evaporation and pyrolysis of Pb^{2+}/Cr^{3+}

View Article Online
DOI: 10.1039/D5SC08541A

precursor solution, it was observed that the presence of culture dish covering enables the precursor solution to convert into uniform colloid and film gradually, relative to the absence of culture dish covering (**Fig. S2**). The morphology and thickness differences between $PbCrO_4$-R_{VCr} and $PbCrO_4$-F_{VCr} films suggested that the formation of $PbCrO_4$ film was significantly impacted by culture dish covering above the Pb^{2+}/Cr^{3+} precursor solution during thermal treating. In further XRD detections, the typical diffraction peaks of monoclinic $PbCrO_4$ (PDF#: 08-0209) were clearly observed for two types of $PbCrO_4$ films, in addition to the signals of FTO substrate (SnO_2, PDF#:46-1088) (**Fig. 2h**). Significantly, the (120) diffraction peak intensity of $PbCrO_4$-F_{VCr} films was 1.26 times as that of $PbCrO_4$-R_{VCr} films. According to the XRD data, the crystallinity of $PbCrO_4$-F_{VCr} films was found to be 85.58%, which is higher than that of $PbCrO_4$-R_{VCr} films (80.41%) (**Table 1**). It is generally believed that the crystallinity of metal oxides is closely influenced by the content of defects. [15] The crystallinity difference implied that the defects' content in $PbCrO_4$-R_{VCr} and $PbCrO_4$-F_{VCr} films is different.

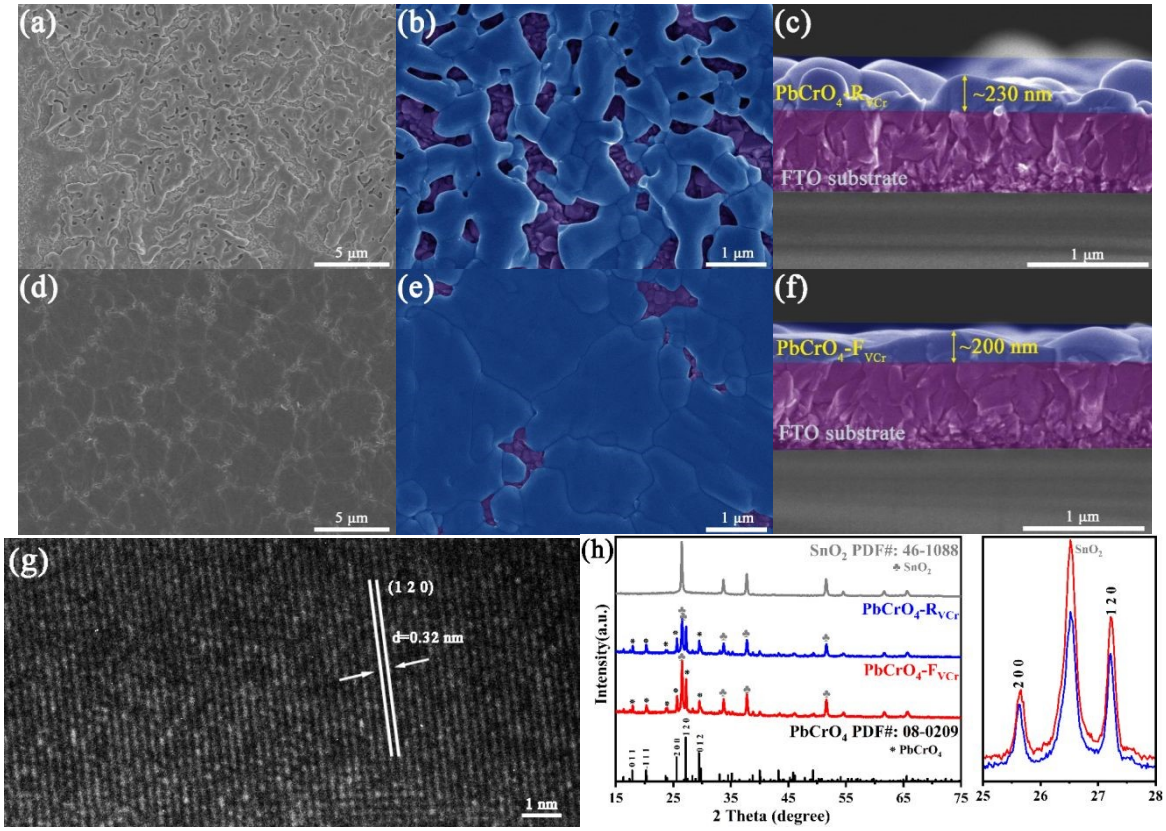

View Article Online
DOI: 10.1039/D5SC08541A

Fig. 2 SEM images of (a-c) $PbCrO_4$-R_{VCr} and (d-f) $PbCrO_4$-F_{VCr} films. (g) HRTEM image of $PbCrO_4$-F_{VCr} films. (h) XRD pattern of $PbCrO_4$-R_{VCr} and $PbCrO_4$-F_{VCr} films.

Table 1 The crystallinity of $PbCrO_4$-R_{VCr} and $PbCrO_4$-F_{VCr} films.

Sample	*hkl*	*2Θ*	*FWHM*	Crystallinity (%)
$PbCrO_4$-F_{VCr} films	(200)	25.636	0.156	85.58
	(120)	27.223	0.133	
$PbCrO_4$-R_{VCr} films	(200)	25.624	0.118	80.41
	(120)	27.218	0.107	

To know the element chemical states of two types of films, $PbCrO_4$-R_{VCr} and $PbCrO_4$-F_{VCr} films were further investigated using XPS. In survey spectrum, the XPS signals of O 1s, Pb 4f and Cr 2p were clearly detected on $PbCrO_4$-R_{VCr} and $PbCrO_4$-F_{VCr} films (**Fig. S3**). In the high-resolution Pb 4f spectrum of two types of $PbCrO_4$ films, the binding energy peaks at 138.27 and 143.12 eV were in good agreement with the Pb^{2+} in monoclinic $PbCrO_4$ (**Fig. 3a**).[27, 28] For the high-resolution Cr 2p spectrum, the binding energy peaks of $PbCrO_4$-R_{VCr} and $PbCrO_4$-F_{VCr} films generally matched the Cr 2p signals in monoclinic $PbCrO_4$ (**Fig. 3b**).[29, 30] However, the Cr 2p binding energy peaks of $PbCrO_4$-R_{VCr} films (578.67 eV, 587.92 eV) negatively shifted relative to $PbCrO_4$-F_{VCr} films (578.87 eV, 588.12 eV), hinting that their Cr have slightly different chemical states. Meanwhile, more obvious oxygen vacancies signals were found in the high-resolution O 1s spectrum of $PbCrO_4$-R_{VCr} films in comparison with $PbCrO_4$-F_{VCr} films, in addition to their similar lattice oxygen and adsorbed oxygen signals (**Fig. 3c**). Taking into account the Cr 2p and O 1s XPS differences between $PbCrO_4$-R_{VCr} and $PbCrO_4$-F_{VCr} films, it can be inferred that $PbCrO_4$-R_{VCr} films contain more defects than $PbCrO_4$-F_{VCr} films. To detect the specific defects in $PbCrO_4$-R_{VCr} and $PbCrO_4$-F_{VCr} films, their EPR spectrum was contrastively recorded. As shown in **Fig. 3d, e** and **f**, two signal centers at g=2.003

and g=3.883 are appeared on two types of $PbCrO_4$ films, which are the typical EPR signals of oxygen vacancies and Cr defects, respectively.[31-34] In comparison, the EPR signals of Cr defects were much stronger than those of oxygen vacancies, indicating that Cr defects are the main defects in $PbCrO_4$-R_{VCr} and $PbCrO_4$-F_{VCr} films and oxygen vacancies are companion species. Obviously, $PbCrO_4$-R_{VCr} films had stronger Cr defects and oxygen vacancies signals than $PbCrO_4$-F_{VCr} films, indicating higher content of Cr defects in $PbCrO_4$-R_{VCr} films. For the preparation of two types of $PbCrO_4$ films, the only condition difference was the presence and absence of culture dish covering above the Pb^{2+}/Cr^{3+} precursor solution during annealing treatment. From above characterizations, it can be known that $PbCrO_4$ films with few Cr defects can be prepared through culture dish covering above the Pb^{2+}/Cr^{3+} precursor solution to reduce the loss of Cr during thermal treating.

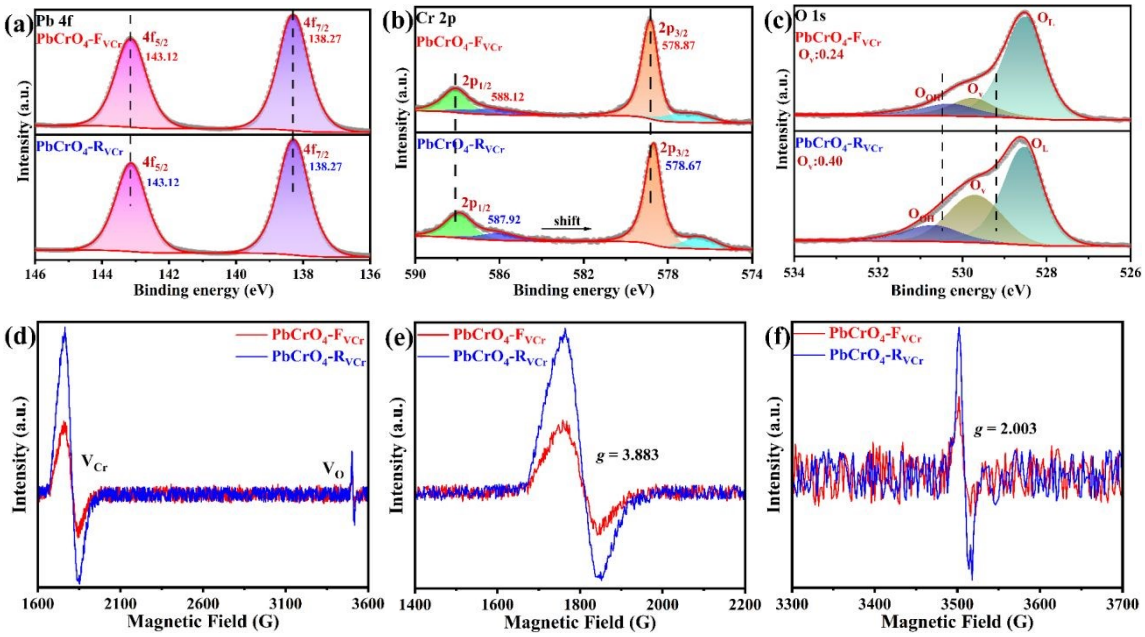

Fig. 3 High-resolution XPS spectra of (a) Pb 4f, (b) Cr 2p and (c) O 1s of $PbCrO_4$-R_{VCr} and $PbCrO_4$-F_{VCr} films. (d-f) EPR spectra of $PbCrO_4$-R_{VCr} and $PbCrO_4$-F_{VCr} films.

3.2 $PbCrO_4$-R_{VCr} and $PbCrO_4$-F_{VCr} films as photoanodes for solar water oxidation.

In previous reports, $PbCrO_4$ films have been demonstrated to work as photoanodes for

View Article Online
DOI: 10.1039/D5SC08541A

solar water oxidation in PBS solution, and their activity can be directly reflected in the magnitude of photocurrent.[4, 6] To check the influence of Cr defects on the solar water oxidation activity of $PbCrO_4$ photoanodes, the photocurrent of two types of $PbCrO_4$ films was measured in 0.5 M PBS under AM 1.5 G irradiation. As shown in **Fig. 4a** and **S4**, higher photocurrent be produced on $PbCrO_4$-F_{VCr} films than $PbCrO_4$-R_{VCr} films. At 1.23 V *vs.* RHE, $PbCrO_4$-F_{VCr} films had a higher photocurrent of 1.13 mA cm^{-2} than $PbCrO_4$-R_{VCr} films (0.55 mA cm^{-2}), indicating their higher solar water oxidation activity. In ABPE measurement, the higher activity was further observed on $PbCrO_4$-F_{VCr} film photoanodes, their maximum ABPE (0.073%) was nearly double for that of $PbCrO_4$-R_{VCr} film photoanodes (0.038%) (**Fig. 4b**). It is important to note that the $PbCrO_4$-F_{VCr} films in the present work have impressive activity compared with recently reported $PbCrO_4$ films (**Table S1**). In η_{sep} detections, $PbCrO_4$-F_{VCr} and $PbCrO_4$-R_{VCr} film photoanodes were found to have η_{sep} of 65% and 45% at 1.23 V *vs.* RHE, respectively (**Fig. 4c**). Meanwhile, the η_{inj} of $PbCrO_4$-F_{VCr} and $PbCrO_4$-R_{VCr} film photoanodes were 29% and 21% at 1.23 V vs RHE, respectively (**Fig. 4d**). Taking the η_{sep} and η_{inj} differences between two types of $PbCrO_4$ film photoanodes as comparisons, it can be found that $PbCrO_4$-F_{VCr} and $PbCrO_4$-R_{VCr} film photoanodes had more significant difference in charge separation than charge injection. The η_{sep} and η_{inj} results suggested that $PbCrO_4$ films with fewer Cr defects can achieve charge separation more effectively.[35] From the morphology observations shown in **Fig. 2a** to **f**, $PbCrO_4$-R_{VCr} films appear to have larger specific surface area than $PbCrO_4$-F_{VCr} films, due to the presence of more gaps. But electrochemical active surface areas (ECSA) testing showed that $PbCrO_4$-F_{VCr} films have larger ECSA (10.31) than $PbCrO_4$-R_{VCr} films (8.60) (**Fig. 4e** and **S6).** In addition, higher electrochemical water oxidation activity was observed on $PbCrO_4$-F_{VCr} films than $PbCrO_4$-R_{VCr} films in dark condition (**Fig. S7**). In term of the electron configuration feature of transition metal electrocatalysts,

View Article Online
DOI: 10.1039/D5SC08541A

[36] Cr would have higher catalytic activity for water splitting than Pb, since Cr has a half-filled 3d orbital ($1s^2 2s^2 2p^6 3s^2 3p^6 3d^5 4s^1$) to provide active sites for reaction while Pb has a full-filled 3d and 5d orbitals ($1s^2 2s^2 2p^6 3s^2 3p^6 4s^2 3d^{10} 4p^6 5s^2 4d^{10} 5p^6 6s^2 4f^{14} 5d^{10} 6p^2$).[37] Therefore, it can be understood that $PbCrO_4$ with more Cr defects have lower electrochemical activity for water oxidation. Based on the photocurrent and ECSA data, it was found that $PbCrO_4$-F_{VCr} films be of higher ECSA-normalized photocurrent than $PbCrO_4$-R_{VCr} films (**Fig. 4f**). Above findings jointly demonstrated that $PbCrO_4$ films with fewer Cr defects can work as higher activity photoanodes for solar water splitting.

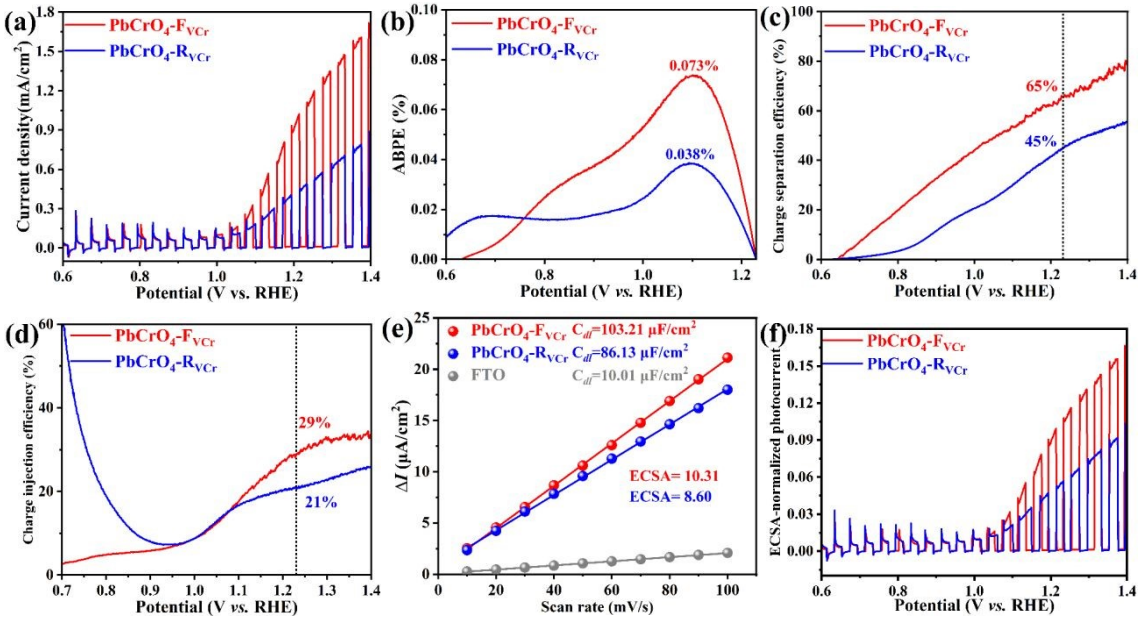

Fig. 4 (a) Chopped LSV curves, (b) ABPE, (c) η_{sep}, (d) η_{inj}, (e) ECSA, and (f) ECSA-normalized photocurrent of $PbCrO_4$-R_{VCr} and $PbCrO_4$-F_{VCr} film photoanodes in 0.5 M PBS.

To get insight into the water oxidation kinetics on two types of $PbCrO_4$ film photoanodes, their Nyquist and Bode plots at 1.23 V *vs.* RHE in 0.5 M PBS under AM 1.5 G irradiation were recorded. As displayed in **Fig. 5a**, the Nyquist plot of $PbCrO_4$-F_{VCr} film photoanodes had smaller arc than that of $PbCrO_4$-R_{VCr} film photoanodes, suggesting faster kinetics in solar water oxidation. Data fitting indicated that the charge transfer (*Rsc*) and water oxidation (*Rct*) resistance on $PbCrO_4$-F_{VCr} film photoanodes was 290 Ω and

View Article Online
DOI: 10.1039/D5SC08541A

186 Ω, respectively (**Table 2**). [38, 39] By comparison, $PbCrO_4$-R_{VCr} film photoanodes had higher *Rsc* (1253 Ω) and *Rct* (962 Ω). Based on the fitted components' values of equivalent circuit, $PbCrO_4$-F_{VCr} film photoanodes were found to have higher k_{O2} and k_{tran} (k_{O2}: 40.6 s^{-1}; k_{tran}: 63.3 s^{-1}) than $PbCrO_4$-R_{VCr} film photoanodes (k_{O2}: 8.2 s^{-1}; k_{tran}: 40.6 s^{-1}) (**Fig. 5b**), indicating faster water oxidation and charge transfer rate on $PbCrO_4$-F_{VCr} film photoanodes. According to the Bode plots, the holes' lifetime (τ) on $PbCrO_4$-F_{VCr} and $PbCrO_4$-R_{VCr} film photoanodes was calculated to be 0.13 ms and 0.34 ms, respectively (**Fig. 5c**). These outcomes confirmed that the holes on $PbCrO_4$-F_{VCr} film photoanodes can react with H_2O molecules quickly in kinetics.[40,41] As previously analyzed, Cr has a half-filled 3d orbital that could provide active sites for water oxidation. Therefore, it is not surprising that $PbCrO_4$ film photoanodes with fewer Cr defects are kinetically favorable for solar water oxidation.

In term of the stability for solar water oxidation, it was unfortunate that unsatisfactory activity decay be observed on $PbCrO_4$-F_{VCr} and $PbCrO_4$-R_{VCr} film photoanodes in 0.5 M PBS during continuous testing at 1.23 V *vs.* RHE (**Fig. S8**). Further investigations found that dissolution and photocorrosion issues are the main causes of activity decay on two types of $PbCrO_4$ film photoanodes in 0.5 M PBS (please see the result discussions for **Fig. S9** to **S11**, and **Table S2** in *Supplementary Information*). According to these findings, the PEC stability testing for $PbCrO_4$-F_{VCr} and $PbCrO_4$-R_{VCr} films was conducted in 0.1 M KHP/0.05M Na_2SO_3 aqueous solution at 1.23 V *vs.* RHE. As shown in **Fig. 5d** and **e,** $PbCrO_4$-F_{VCr} films have higher photocurrent than $PbCrO_4$-R_{VCr} films, showing their higher activity for SO_3^{2-} oxidation. After 3000 s of continuous reaction, 90.0% activity was retained on $PbCrO_4$-F_{VCr} films, while $PbCrO_4$-R_{VCr} films was 70.3% (**Fig. 5e**). Contrastive XRD, Raman and SEM investigations indicated that the crystalline phases, molecular structure and morphology of two types of $PbCrO_4$ film photoanodes have slight

View Article Online
DOI: 10.1039/D5SC08541A

change after stability testing (**Fig. 5f** and **S10, S11**). However, $PbCrO_4$-R_{VCr} films after stability testing had more pronounced decrease in their XRD peaks' intensity, relative to $PbCrO_4$-F_{VCr} films (**Fig. 5f**). From the stability difference between $PbCrO_4$-F_{VCr} and $PbCrO_4$-R_{VCr} film photoanodes, it can be known that $PbCrO_4$ with fewer Cr defects is more stable to drive PEC reactions.

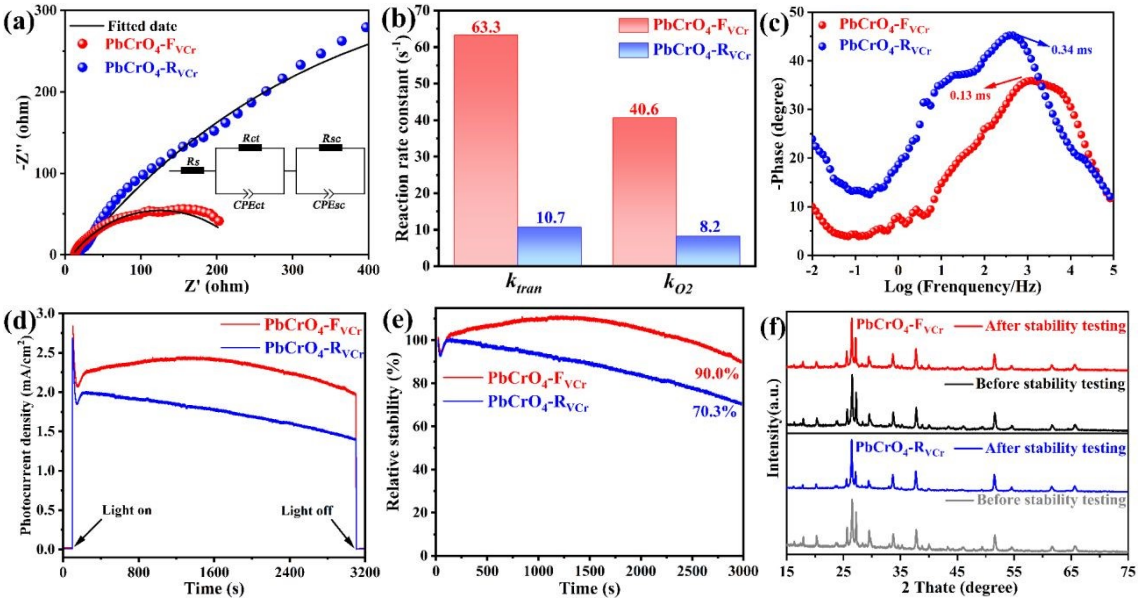

Fig. 5 (a) Nyquist plots, (b) Reaction rate constants, (c) Bode plots for $PbCrO_4O_4$-R_{VCr} and $PbCrO_4$-F_{VCr} film photoanodes in 0.5 M PBS at 1.23 V *vs.* RHE under AM 1.5 G irradiation. (d) *j-t* curves and (e) photocurrent change rate of $PbCrO_4O_4$-R_{VCr} and $PbCrO_4$-F_{VCr} film photoanodes in 0.1M KHP/0.05M Na_2SO_3 at 1.23 V *vs.* RHE under AM 1.5 G irradiation. (f) XRD patterns of $PbCrO_4O_4$-R_{VCr} and $PbCrO_4$-F_{VCr} films before and after the stability testing.

Table 2 The fitted components' values for the equivalent circuit of two types of $PbCrO_4$ film photoanodes (inset of **Fig. 5a**).

Sample	R_s/Ω (error)	R_{ct}/Ω (error)	CPE_{ct}/F (error)	R_{sc}/Ω (error)	CPE_{sc}/F (error)
$PbCrO_4$-R_{VCr}	17.67 (1.98%)	962 (6.26%)	9.72E-5 (5.15%)	1253 (4.39%)	1.50E-4 (7.20%)
$PbCrO_4$-F_{VCr}	10.67 (1.42%)	186 (2.62%)	8.47E-5 (5.23%)	290 (7.93%)	2.80E-4 (7.62%)

View Article Online
DOI: 10.1039/D5SC08541A

3.2 The mechanism of $PbCrO_4$ films with fewer Cr defects being of higher activity

Above investigations demonstrated that $PbCrO_4$ films with fewer Cr defects have higher solar water oxidation activity. To reveal the mechanism of $PbCrO_4$ films with fewer Cr defects being of higher activity, the physicochemical properties of $PbCrO_4$-F_{VCr} and $PbCrO_4$-R_{VCr} films involving solar water oxidation were contrastively checked. First of all, the UV-vis light absorption property of two types of $PbCrO_4$ films was investigated. As shown in **Fig. 6a**, $PbCrO_4$-F_{VCr} and $PbCrO_4$-R_{VCr} films have a close absorption edge around 550 nm, which corresponds to the typical band gap of monoclinic $PbCrO_4$ (~2.2 eV). [1, 42] Meanwhile, the light absorption intensity of two types of $PbCrO_4$ films was very close too, and the absorbed photon flux of $PbCrO_4$-F_{VCr} and $PbCrO_4$-R_{VCr} films was 7.03 mA cm^{-2} and 7.08 mA cm^{-2}, respectively **(Fig. 6b)**. These observations indicated that the obvious activity difference between $PbCrO_4$-F_{VCr} and $PbCrO_4$-R_{VCr} films not be caused by their difference in light absorption property. In PL spectrum investigations, weaker PL peak intensity was detected on $PbCrO_4$-F_{VCr} films compared with $PbCrO_4$-R_{VCr} films, reflecting lower carrier recombination in/on $PbCrO_4$-F_{VCr} films **(Fig. 6c)**. In addition, stronger surface photovoltage signals were detected on $PbCrO_4$-F_{VCr} films than $PbCrO_4$-R_{VCr} films, further confirming better carrier separation and transfer in/on $PbCrO_4$-F_{VCr} films **(Fig. 6d** and **S12)**. As mentioned in *Introduction* that the presence of high-concentration Cr defects in monoclinic $PbCrO_4$ could disrupt its CrO_4 tetrahedron network and form defect-level traps, which are disadvantageous to the delocalization separation and transfer of electrons/holes in theory. To confirm the effect of Cr defects on carrier separation and transfer, the open-circuit potential (OCP) variations were detected on $PbCrO_4$-F_{VCr} and $PbCrO_4$-R_{VCr} films under and without AM 1.5G irradiation. As displayed in **Fig. 6e**, an OCP_{light} of ~0.461 V *vs.* RHE be observed on two types of $PbCrO_4$ films, while the OCP_{dark} of $PbCrO_4$-F_{VCr} and $PbCrO_4$-R_{VCr} films is 0.582 and

View Article Online
DOI: 10.1039/D5SC08541A

0.552 V *vs.* RHE, respectively. Accordingly, more obvious OCP variation was produced on $PbCrO_4$-F_{VCr} films (0.123 V) than $PbCrO_4$-R_{VCr} films (0.098 V), suggesting that $PbCrO_4$ films with fewer Cr defects have better charge separation and transfer properties.[43, 44] In the Mott-Schottky plots **(Fig. 6f)**, a more negative E_{fb} of 0.12 V *vs.* RHE was observed on $PbCrO_4$-F_{VCr} films, relative to $PbCrO_4$-R_{VCr} films (0.15 V). Considering the relevance of E_{fb} in n-type semiconductors to their Fermi level position (E_f), $PbCrO_4$-F_{VCr} films being of more negative E_{fb} indicates that $PbCrO_4$ with fewer Cr defects has higher E_f and carrier concentration ($PbCrO_4$-F_{VCr} films: 1.98×10^{19} cm^{-3}; $PbCrO_4$-R_{VCr} films: 1.51×10^{19} cm^{-3}).

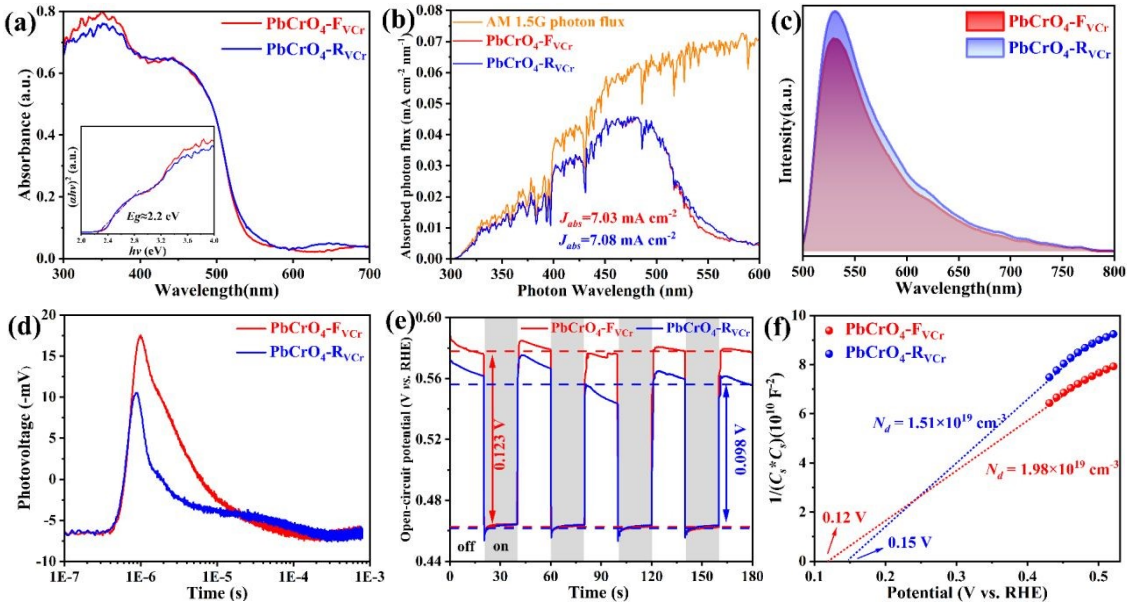

Fig. 6 (a) UV-vis absorption spectra, (b) absorbed photon flux, (c) PL spectra, (d) transient photovoltage spectra of $PbCrO_4$-R_{VCr} and $PbCrO_4$-F_{VCr} films in air. (e) OCP variations and (f) Mott-Schottky plots of $PbCrO_4$-R_{VCr} and $PbCrO_4$-F_{VCr} films in 0.5 M PBS under AM 1.5 G irradiation.

In term of chargeability, one Cr^{6+} defect carries three effective negative charges (V_{Cr}''') in monoclinic $PbCrO_4$. From unit cell structural perspective, the presence of Cr defects could cause the formation of unsaturated O dangling bonds on $PbCrO_4$ surface. To check the presence and content difference of O dangling bonds on two types of $PbCrO_4$ films,

View Article Online
DOI: 10.1039/D5SC08541A

their hydrophilicity was contrastively detected (**Fig. 7a**). Interestingly, weaker hydrophilicity was observed on $PbCrO_4$-R_{VCr} films (θ=35.4˚) relative to $PbCrO_4$-F_{VCr} films (θ=10.2˚), although $PbCrO_4$-R_{VCr} films had rougher surface (SEM images shown in **Fig. 2a** to **2f**). In essence, the hydrophilicity of film depends on the interaction intensity between H_2O molecules and surface compound.[45] It has been reported that high-concentration Al defects in α-Al_2O_3 can result in the reconstitution of unsaturated O dangling bonds and the decrease of surface energy, thereby α-Al_2O_3 with rich Al defects has weaker hydrophilicity than pristine α-Al_2O_3.[46] The hydrophilicity difference suggested that $PbCrO_4$-F_{VCr} and $PbCrO_4$-R_{VCr} films have different content of O dangling bonds on surface, owing to their difference in Cr defects content. The presence of O dangling bonds usually has negative effect on carrier separation on semiconductors' surface.[47, 48] Through the -SH groups of 1-octadecanethiol passivated the O dangling bonds on $PbCrO_4$ films,[49-51] the photocurrent of $PbCrO_4$-R_{VCr} films was found to increase by 62%, but only 24% increase on $PbCrO_4$-F_{VCr} films (**Fig. 7b** and **7c**). The photocurrent enhancement on 1-octadecanethiol-passivated $PbCrO_4$ films confirmed the presence of O dangling bonds and the negative effect of O dangling bonds on carrier separation on $PbCrO_4$. Meanwhile, more obvious photocurrent improvement on 1-octadecanethiol-passivated $PbCrO_4$-R_{VCr} films reflected their higher content of O dangling bonds, due to rich Cr defects.

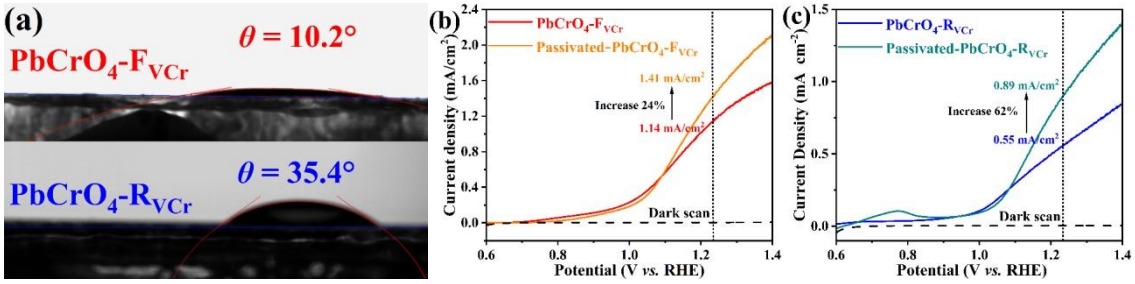

Fig. 7 (a) Water contacting angle images of $PbCrO_4$-F_{VCr} and $PbCrO_4$-R_{VCr} films. In 0.5 M PBS under AM 1.5 G irradiation, LSV curves of (b) $PbCrO_4$-F_{VCr} and (c) $PbCrO_4$-R_{VCr} films before and after 1-octadecanethiol passivating.

View Article Online
DOI: 10.1039/D5SC08541A

To understand the influence of Cr defects on the band structure and carrier localization of $PbCrO_4$, the density of states and electron localization function of monoclinic $PbCrO_4$ with and without Cr defects were simulated by DFT calculations. As shown in **Fig. 8a**, $PbCrO_4$ and $PbCrO_4$-V_{Cr} had similar total density of state (TDOS), indicating that their theoretical carrier density is relatively close. From the density of state (PDOS) (**Fig. 8b** and **c**), the valence and conduction band of $PbCrO_4$ and $PbCrO_4$-V_{Cr} can be observed to be mainly composed of O 2p and Cr 3d orbital, respectively. However, two small peaks corresponding O 2p and Cr 3d orbital were found at the Fermi level of $PbCrO_4$-V_{Cr} (**Fig. 8c)**, indicating that deep energy level be formed in the band structure of $PbCrO_4$-V_{Cr} due to the presence of Cr defects. The presence of deep energy level in $PbCrO_4$ with Cr defects was actually reflected in the surface photovoltage spectrum of $PbCrO_4$-R_{VCr} films (shown in **Fig. 6d**), in which small photovoltage trailing in the time scale of 10^{-5}~10^{-4} s was displayed. It has been reported that the formation of deep energy level in semiconductors usually results in high non-radiative recombination of carrier. [52,53] In term of structure theory, the presence of Cr defects in $PbCrO_4$ could trigger strong non-radiative recombination of carrier, since the d-d transition of Cr^{6+} is limited by spin selectivity and its radiation rate is low. Electron localization comparisons suggested that the presence of Cr defects increases the localization degree of carrier in $PbCrO_4$ (**Fig. 8d**), hinting the negative impact of Cr defects on carrier transfer in $PbCrO_4$.[54,55] Combined with the experimental findings of higher carrier recombination in/on $PbCrO_4$-R_{VCr} films than $PbCrO_4$-F_{VCr} films (**Fig. 6c** and **d**), it is certain that the presence of Cr defects in $PbCrO_4$ can result in the formation of deep energy level which is not conducive to carrier transfer in the bulk of $PbCrO_4$.

View Article Online
DOI: 10.1039/D5SC08541A

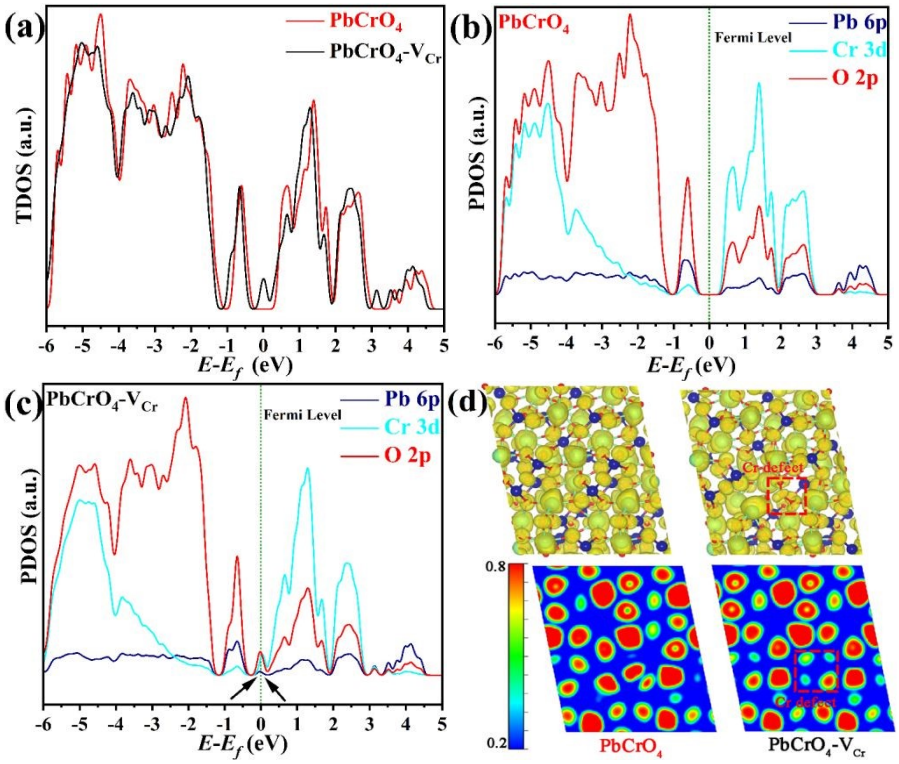

Fig. 8 (a) Total density of states, (b, c) partial density of states, and (d) electron localization function of $PbCrO_4$ with and without Cr defects.

The Gibbs free energy (ΔG) of water oxidation on $PbCrO_4$ with and without Cr defects was further simulated by DFT calculations based on typical four-electron pathway (***Reactions*** **(1)** to **(4)**). [56, 57]

$$H_2O(l)+*\rightarrow *OH+H_2O_2+H^++e^- \quad (1)$$

$$*OH+H_2O(l)+H^++e^-\rightarrow *O+H_2O(l)+2H^++2e^- \quad (2)$$

$$*O+2H_2O(l)+2H^++2e^-\rightarrow *OOH+3H^++3e^- \quad (3)$$

$$*OOH+3H^++3e^-\rightarrow O_2+4H^++4e^- \quad (4)$$

For the adsorption of H_2O on $PbCrO_4$, it was observed that H_2O molecules preferentially adsorbed on the Cr sites of $PbCrO_4$ (**Fig. 9a**), since Cr has a half-filled 3d orbital to provide active sites. [36] The adsorption energy of H_2O molecules on $PbCrO_4$ was -2.034 eV, which is more negative than that on $PbCrO_4$-V_{Cr} (-1.564 eV). $PbCrO_4$ being of more negative H_2O adsorption energy means that $PbCrO_4$ has better property for H_2O

View Article Online
DOI: 10.1039/D5SC08541A

adsorption than $PbCrO_4$-V_{Cr}, which is consistent with the hydrophilicity results shown in **Fig. 7a**. For water oxidation, strong H_2O adsorption on photoanodes is energetically favorable to the subsequent dissociation.[58-61] In subsequent calculations for the dehydrogenation of H_2O into O_2 on $PbCrO_4$ and $PbCrO_4$-V_{Cr}, different ΔG was found in each elementary steps (**Fig. 9b** to **d**). Significantly, the rate-limiting step of water oxidation on $PbCrO_4$-V_{Cr} was found to be the dehydrogenation of *OH into *O and its energy barrier was 1.88 eV. For $PbCrO_4$, its rate-limiting step of water oxidation was the reaction of *OH with H_2O to form *OOH and its energy barrier was 1.61 eV. This comparison indicates that the presence of Cr defects turns the rate-limiting step of water oxidation on $PbCrO_4$ to the dehydrogenation of *OH into *O which requires a higher energy barrier of 1.88 eV. Based on the EIS experimental results (**Fig. 5a** to **c, Table 2**), it can be further known that the presence of Cr defects weakens the catalytic activity of $PbCrO_4$ for water oxidation, and turns the rate-limiting step to the dehydrogenation of *OH into *O that requires a high energy barrier of 1.88 eV. Considering the negative effect of Cr defects and the easy formation of Cr defects in $PbCrO_4$ films using drop-coating/thermal treating approach, we discovered that $PbCrO_4$ films with higher water oxidation activity can be prepared by using slightly excessive of Cr precursor to compensate the loss of Cr in thermal treating, in addition culture dish covering precursor solution. As shown in **Fig. 9e** and **f**, highest water oxidation photocurrent was achieved on the $PbCrO_4$ films that were prepared using the precursor solution with Pb/Cr atomic ratio=100.0/100.7. Meanwhile, the $PbCrO_4$ film prepared with Pb/Cr atomic ratio=100.0/100.7 had the highest crystallinity (86.11%) (**Fig. S13** and **Table S3**). Above finding provides a solution for the preparation of high-activity $PbCrO_4$ films.

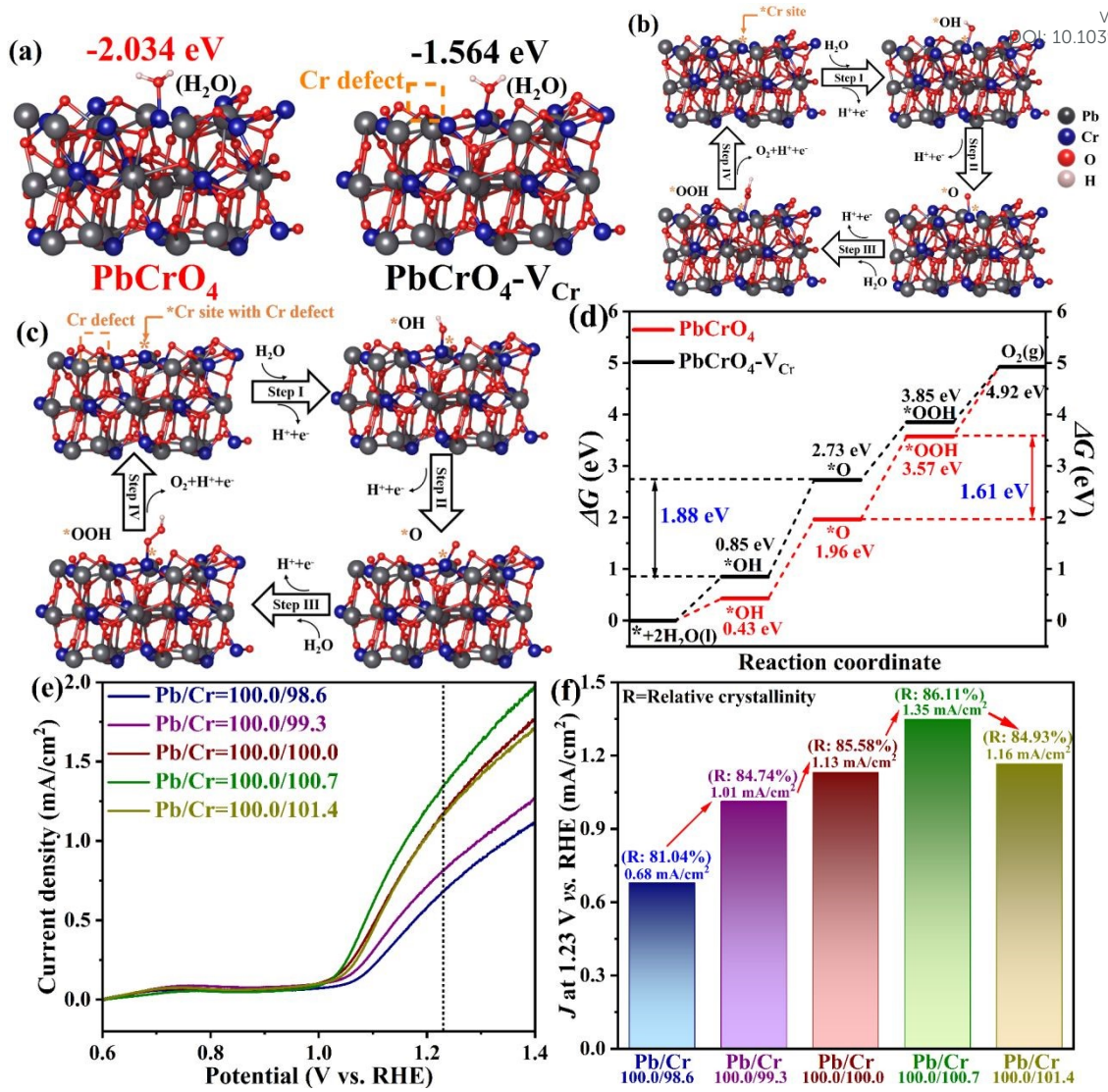

Fig. 9 (a) Adsorption configuration of H_2O on $PbCrO_4$ with and without Cr defects. Intermediate configuration of water oxidation on $PbCrO_4$ (b) with and (c) without Cr defects. (d) Free energy diagrams for water oxidation on $PbCrO_4$ with and without Cr defects at U=0, pH=0 and T=298 K. (e) LSV curves and (f) water oxidation photocurrent at 1.23 V vs. RHE of $PbCrO_4$ films prepared using different Pb/Cr atomic ratios.

Summarized the findings from experimental detections and theoretical calculations, the mechanism of $PbCrO_4$ films with fewer Cr defects being of higher activity can be explained as following: (i) the presence of Cr defects results in the formation of deep energy level in $PbCrO_4$, which is unfavorable to carrier transfer in the bulk of $PbCrO_4$ films; (ii) the presence of Cr defects causes the formation of unsaturated O dangling bonds on $PbCrO_4$, which are harmful traps for carrier separation on the surface of $PbCrO_4$ films;

View Article Online
DOI: 10.1039/D5SC08541A

(iii) Cr has a half-filled $3d^5$ orbital to provide active sites for reaction, the presence of Cr defects weakens the catalytic activity of $PbCrO_4$ for water oxidation, and turns the rate-limiting step to the dehydrogenation of *OH into *O which requires a high energy barrier of 1.88 eV.

4 Conclusions

In summary, monoclinic $PbCrO_4$ films with few Cr defects ($PbCrO_4$-F_{VCr}) were prepared on FTO substrate through covering the drop-coating Pb^{2+}/Cr^{3+} precursor solution to reduce the thermal loss of Cr during annealing treatment. Compared with the monoclinic $PbCrO_4$ films with rich Cr defects ($PbCrO_4$-R_{VCr}), the $PbCrO_4$-F_{VCr} films as photoanodes had higher solar water oxidation activity. A higher water oxidation photocurrent of 1.13 mA cm^{-2} at 1.23 V *vs.* RHE was produced on the $PbCrO_4$-F_{VCr} film photoanodes, while the $PbCrO_4$-R_{VCr} film photoanodes was 0.55 mA cm^{-2}. Meanwhile, faster water oxidation kinetics was found on the $PbCrO_4$-F_{VCr} film photoanodes, relative to the $PbCrO_4$-R_{VCr} film photoanodes. The $PbCrO_4$-F_{VCr} film photoanodes had a water oxidation rate constant (k_{O2}) of 40.6 s^{-1}, and the k_{O2} of $PbCrO_4$-R_{VCr} film photoanodes was 8.2 s^{-1}. $PbCrO_4$ films with fewer Cr defects being of higher solar water oxidation activity can be attributed to following reasons: (i) the presence of Cr defects can result in the formation of deep energy level in $PbCrO_4$, which is unfavorable to carrier transfer in the bulk of $PbCrO_4$ films; (ii) the presence of Cr defects can cause the formation of unsaturated O dangling bonds on $PbCrO_4$, which are harmful traps for carrier separation on the surface of $PbCrO_4$ films; (iii) Cr has a half-filled $3d^5$ orbital to provide active sites for reaction, the presence of Cr defects weakens the catalytic activity of $PbCrO_4$ for water oxidation, and turns the rate-limiting step to the dehydrogenation of *OH into *O which requires a high energy barrier of 1.88 eV. The present work provides insight into

monoclinic $PbCrO_4$ film photoanodes from the relevance of preparation condition, Cr defects, water oxidation activity and reaction mechanism.

Notes

The authors declare no competing financial interest.

Acknowledgements

This work was supported by National Natural Science Foundation of China (41702037), Natural Science Foundation of Chongqing (No. CSTB2023NSCQ-MSX0765), and Research Foundation of Chongqing University of Science and Technology (ckrc2022003).

References

1. A. E. Lindberg, W. Wang, S. Zhang, G. Galli and K. S. Choi, *ACS Appl. Energy Mater.*, 2020, **3**, 8658- 8666.
2. H. C. Lee, S. K. Cho, H. S. Park, K. M. Nam and A. J. Bard, *J. Phys. Chem. C*, 2017, **121**, 17561- 17568.
3. S. K. Cho, R. Akbar, J. Kang, W. Lee and H. S. Park, *J. Mater. Chem. A*, 2018, **6**, 13312- 13320.
4. H. Zhou, D. Zhang, X. Gong, Z. Feng, M. Shi, Y. Liu, C. Zhang, P. Luan, P. Zhang, F. Fan, R. Li and C. Li, *Adv. Mater.*, 2022, **34**, 2110610.
5. Y. R. Gwon, J. Kang, S. Choe and S. K. Cho, *J. Electrochem. Soc.*, 2023, **170**, 106504.
6. H. Zhou, D. Zhang, H. Xie, Y. Liu, C. Meng, P. Zhang, F. Fan, R. Li and C. Li, *Adv. Mater.*, 2023, **35**, 2300914.
7. J. Kang, Y. R. Gwon and S. K. Cho, *J. Electroanal. Chem.*, 2020, **878**, 114601.
8. M. G. Walter, E. L. Warren, J. R. McKone, S. W. Boettcher, Q. Mi, E. A. Santori and N. S. Lewis, *Chem. Rev.*, 2010, **110**, 6446- 6473.
9. Y. Zhang and J. Yan, *Chem. Eng. J.*, 2023, **472**, 144831.
10. J. Xiong, J. Di, J. Xia, W. Zhu and H. Li, *Adv. Funct. Mater.*, 2018, **28**, 1801983.
11. H. Effenberger and F. Pertlik, *Z. Kristallogr.*, 1986, **176**, 75
12. D. Errandonea, A. Muñoz, P. Rodríguez-Hernández, J. E. Proctor, F. Sapiña and M.

View Article Online
DOI: 10.1039/D5SC08541A

Bettinelli, *Inorg. Chem.*, 2015, **54**, 7524- 7535.

13. M. Lamers, S. Fiechter, D. Friedrich, F. F. Abdi and R. van de Krol, *J. Mater. Chem. A*, 2018. **6**, 18694- 18700.
14. T. K. van Leeuwen, R. Dowdy, A. Guerrero and P. Gannon, *J. Power Sources.*, 2023, **572**, 233065.
15. K. Chen, X. Yuan, Z. Tian, M. Zou, Y. Yuan, Z. Chen, Q. Zhang, Y. Zhang, X. Jin, T. Wu, R. Shahbazian-Yassar and G. Liu, *Nat. Mater.*, 2025, **24**, 835- 842.
16. H. Kato, K. Asakura and A. Kudo, *J. Am. Chem. Soc.*, 2003, **125**, 3082- 3089.
17. K. Sivula, R. Zboril, F. Le Formal, R. Robert, A. Weidenkaff, J. Tucek, J. Frydrych and M. Grätzel, *J. Am. Chem. Soc.*, 2010, **132**, 7436- 7444.
18. J. Xiao, L. Fan, F. Zhao, Z. Huang, S. F. Zhou and G. Zhan, *J. Catal.*, 2020, **381**, 139- 149.
19. G. M. Carroll and D. R. Gamelin, *J. Mater. Chem. A*, 2016, **4**, 2986- 2994.
20. J. Zhang, R. García-Rodríguez, P. Cameron and S. Eslava, *Energy Environ. Sci.*, 2018, **11**, 2972- 2984.
21. C. Debraj, K. Ouchi, Y. Tsubonouchi, Z. N. Zahran and M. Yagi, *App. Catal. B: Environ.*, 2026, **380**, 125733.
22. G. Kresse and J. Hafner, *Phys. Rev. B*, 1995, **47**, 558.
23. G. Kresse and J. Hafner, *Phys. Rev. B* 1994, **49**, 14251.
24. J. P. Perdew, K. Burke and M. Ernzerhof, *Phys. Rev. Lett.*, 1996, **77**, 3865.
25. G. Kresse and D. Joubert, *Phys. Rev. B*, 1999, **59**, 1758.
26. S. Grimme, J. Antony, S. Ehrlich and H. Krieg, *J. Chem. Phys.*, 2010, **132**, 154104.
27. H. Abdel-Samad and P. R. Watson, *Appl. Surf. Sci.*, 1998, **136**, 46-54.
28. H. Bi, G. Han, M. Guo, C. Ding, H. Zou, Q. Shen, S. Hayase and W. Hou, *ACS Appl. Mater. Interfaces*, 2022, **14**, 35513-35521.
29. M. C. Biesinger, C. Brown, J. R. Mycroft, R. D. Davidson and N. S. McIntyre, *Surf. Interface Anal.* 2004, **36**, 1550-1563.
30. M. C. Biesinger, B. P. Payne, A. P. Grosvenor, L. W.M. Lau, A. R. Gerson and R. St.C. Smart, *Appl. Surf. Sci.* 2011, **257**, 2717-2730.
31. L. Wang, S. Zhang, X. Lin, Q. Chen and H. Chen, *Chem. Eng. J.* 2024, **481**, 147955.
32. D. Zu, Y. Ying, Q. Wei, P. Xiong, M. S. Ahmed, Z. Lin, M. M. Li, M. Li, Z. Xu, G. Chen, L. Bai, S. She, Y. Tsang and H. Huang, *Angew. Chem. Int. Ed.*, 2024, **63**, e202405756.
33. B. Qu and L. *Chinese J. Lumin.* 2023, **43**, 1815-1822.

View Article Online
DOI: 10.1039/D5SC08541A

34. F. Gan, H. Deng and H. Liu, *J. Non-Cryst. Solids*, **1982**, 52, 135-141.
35. K. Tsai, C. Lai, Y. Chen, Leu, Ing-Chi, J. Chang, C. Kuo, S. Tseng, Y. Li and Y. Pu, *App. Catal. B: Environ.*, 2024, **341**, 123288.
36. L. Han and S. Dong, E. Wang, *Adv. Mater.* 2016, **28**, 9266-9291.
37. J. Chen, H. Li, S. Chen, J. Fei, C. Liu, Z. Yu, K. Shin, Z. Liu, L. Song, H. Graeme, L. Wei and Y. Chen, *Adv. Energy Mater.*, 2021, **11**, 2003412.
38. S. Ye, W. Shi, Y. Liu, D. Li, H. Yin, H. Chi, Y. Luo, N. Ta, F. Fan, X. Wang and C. Li, *J. Am. Chem. Soc.*, 2021, **143**, 12499-12508.
39. W. Nabgan, B. Nabgan, A. A. Jalil, M. Ikram, I. Hussain, M. B. Bahari, T.V. Tran, M. Alhassan, A.H.K. Owgi, L. Parashuram, A. H. Nordin and F. Medina, *Int. J. Hydrogen Energy*, 2024, **52**, 358-380.
40. S. Corby, R. R. Rao, L. Steier and J. R. Durrant, *Nat. Rev. Mater.*, 2021, **6**, 1136-1155.
41. J. Zhang, Y. Deng, D. Gu, S. Wang, L. She, R. Che, Z. S. Wang, B. Tu, S. Xie and D. Zhao, *Adv. Energy Mater.*, 2011, **1**, 241-248.
42. M. Ma, K. Zhang, P. Li, M. S. Jung and M. J. Jeong, *Angew. Chem. Int. Ed.*, 2016, **55**, 11819-11823.
43. K. H. Ye, H. Li, D. Huang, S. Xiao, W. Qiu, M. Li, Y. Hu, W. Mai, H. Ji and S. Yang, *Nat. Commun.*, 2019, **10**, 3687.
44. F. A L. Laskowski, M. R. Nellist, J. Qiu and S. W. Boettcher, *J Am Chem Soc.*, 2019, **141**, 1394-1405.
45. R. J. Good, *J. Adhes. Sci. Technol.*, 1992, **6**, 1269.
46. K. P. D. Lagerlöf and R. W. Grimes, *Acta Mater.*, 1998, **46,** 5689-5700.
47. H. Wang, S. Jiang, H. Yu, K. Deng, Z. Wang, X. Li, Y. Xu and L. Wang, *J. Mater. Chem. A*, 2023, **11**, 13633-13639.
48. X. Zhong, H. He, M. Yang, G. Ke, Z. Zhao, F. Dong, B. Wang, Y. Chen, X. Shi and Y. Zhou, *J. Mater. Chem. A*, 2018, **6**, 10456-10465.
49. M. Yang, H. He, H. Zhang, G. Ke, X. Zhong, F. Dong, Y. Chen, J. Du and Y. Zhou, *Electrochim. Acta*, 2018, **283**, 871-881.
50. G. Yang, Y. Li, Y. Liu, F. Xie, G. Yan, X. Yang, C. Wei, B. Bian, X. Zhang and N. Lu, *IEEE Trans. Electron Devices*, 2022, **69**, 195-200.
51. X. Min, Q. Xie, Z. Wang, X. Wang and M. Chen, *Mater. Chem.*, *Phys.*, 2022, **276**, 125404.
52. J. Ma, H. Chi, A. Wang, P. Wang, H. Jing and T. Yao, *J. Am. Chem. Soc.*, 2022, **144**,

View Article Online
DOI: 10.1039/D5SC08541A

17540-17548.

53. Z. Zhu, K. Mao, K. Zhang, W. Peng, J. Zhang, H. Meng, S. Cheng, T. Li, H. Lin, Q. Chen, X. Wu and J. Xu, *Joule*, 2022, **6**, 2849-2868.
54. S. Wang, L. Pan, J. Song, W. Mi, J. Zou, L. Wang and X. Zhang, *J. Am. Chem. Soc.*, 2015, **137**, 2975-2983.
55. P. Fuentealba, E. Chamorro, J. Santos and A. Toro-Labbé, *Comput. Theor. Chem.*, 2007, **19**, 57-85.
56. S. Wang, T. He, P. Chen, A. Du, K. Ostrikov, W. Huang and L. Wang, *Adv. Mater.*, 2020, **32**, 2001385.
57. M. Gerosa, F. Gygi, M. Govoni and G. Galli, *Nat. Mater.*, 2018, **17**, 1122-1127.
58. P. Li, X. Chen, H. He, X. Zhou, Y. Zhou and Z. Zou, *Adv.Mater.*, 2018, **30**, 1703119.
59. S. Wan, C. Dong, J. Jin, J. Li, Q. Zhong, K. Zhang and J. H. Park, *ACS Energy Lett.*, 2022, **7**, 3024−3031.
60. P. Yue, H. She, L. Zhang, B. Niu, R. Lian, J. Huang, L. Wang and Q. Wang, *App. Catal. B: Environ.*, 2021, **286**, 119875.
61. X. Wei, J. Zhang, L. Wang, Y. Bai, J. Huang, H. She and Q. Wang, *Chem. Eng. J.*, 2024, **482**, 149114.

View Article Online
DOI: 10.1039/D5SC08541A

Data Availability Statement

The data in our manuscript are available from the corresponding author on reasonable request.